Letter

# $s^{\pm}$-wave superconductivity in pressurized $La_4Ni_3O_{10}$

Ming Zhang,[1,*] Hongyi Sun,[2,3,*] Yu-Bo Liu,[4,*] Qihang Liu,[5,6] Wei-Qiang Chen,[5,6,†] and Fan Yang[4,‡]

[1]*Zhejiang Key Laboratory of Quantum State Control and Optical Field Manipulation, Department of Physics, Zhejiang Sci-Tech University, Hangzhou 310018, Zhejiang, China*

[2]*Shenzhen Institute for Quantum Science and Engineering, Southern University of Science and Technology, Shenzhen 518055, China*

[3]*International Quantum Academy, Shenzhen 518048, China*

[4]*School of Physics, Beijing Institute of Technology, Beijing 100081, China*

[5]*Department of Physics and Guangdong Basic Research Center of Excellence for Quantum Science, Southern University of Science and Technology, Shenzhen 518055, China*

[6]*Shenzhen Key Laboratory of Advanced Quantum Functional Materials and Devices, Southern University of Science and Technology, Shenzhen 518055, China*

(Received 1 April 2024; revised 13 October 2024; accepted 18 October 2024; published 4 November 2024)

Recently, evidence of superconductivity (SC) has been reported in pressurized $La_4Ni_3O_{10}$. Here we study its possible pairing mechanism and pairing symmetry. Through fitting the density-functional-theory band structure, we provide a six-orbital tight-binding model. In comparison with the band structure of $La_3Ni_2O_7$, the additional nonbonding $d_{z^2}$ band is important to the pairing mechanism here. When the multiorbital Hubbard interactions are included, our random-phase-approximation based study yields an $s^{\pm}$-wave SC. The dominant Fermi-surface nesting with vector $\mathbf{Q}_1 \approx (\pi, \pi)$ is between the $\gamma$ pocket contributed by the bonding $d_{z^2}$ band top and the $\alpha_1$ pocket contributed by the nonbonding $d_{z^2}$ band bottom, leading to the strongest pairing amplitude and opposite gap signs within the two regimes. The dominant real-space pairing is the interlayer $d_{z^2}$-orbital pairing. This $s^{\pm}$-wave pairing pattern is insensitive to the band details. Upon electron doping, the $T_c$ would increase promptly before the system enters the Néel-ordered spin-density-wave phase.

DOI: 10.1103/PhysRevB.110.L180501

*Introduction*. The recent discovery of superconductivity (SC) in the nickel-based family [1–8], especially the high-temperature SC near 80 K in the bilayer nickelate $La_3Ni_2O_7$ under pressure [9–28], has raised a surge of interest in exploring the electron correlation and pairing nature in this family [29–92]. $La_3Ni_2O_7$ belongs to the Ruddlesden-Popper (RP) phase with formula $La_{n+1}Ni_nO_{3n+1}$ [93,94], which consists of $n$ layers of perovskite-type $LaNiO_3$, separated by a single rocksalt-type LaO layer along the $c$-axis direction. While $n = 2$ is for $La_3Ni_2O_7$, the $n = 3$ member of this family is $R_4Ni_3O_{10}$ ($R$ = La, Pr, Nd). Recently, clear zero resistance and diamagnetism of $La_4Ni_3O_{10}$ under pressure below 20–30 K were observed [95–98], indicating signatures of SC. The maximum $T_c$ of $La_4Ni_3O_{10}$ is lower than $La_3Ni_2O_7$, while its superconducting volume fraction is found to be very high [97], indicating that the superconductivity in $La_4Ni_3O_{10}$ is a bulk property rather than filamentary as in the present-stage $La_3Ni_2O_7$ [18].

$La_4Ni_3O_{10}$ hosts a quasi-2D crystal structure, with approximate unit cell comprising three $NiO_2$ layers interconnected by the Ni-O-Ni $\sigma$ bond. Under high pressure, there is a structural transition from monoclinic $P2_1/a$ to tetragonal $I4/mmm$ [95–108]. It takes the 164.8° Ni-O-Ni angle between adjacent octahedra layers forced to 180.0° in the high-pressure phase, reminiscent of the bilayer $La_3Ni_2O_7$ [9–19]. While the $NiO_2$ plane in $La_4Ni_3O_{10}$ is isostructural with the $CuO_2$ plane in the cuprates, the nominal valence state of Ni is +2.67, leading to the electron configuration $d^{7.33}$, which is different from the $d^9$ state in the cuprates, the $d^7$ state in the infinite-layer nickelates, and the $d^{7.5}$ state in bilayer $La_3Ni_2O_7$. Particularly, the filling fractions of both $3d$ orbitals in $La_4Ni_3O_{10}$ are near $1/3$, which is quite different from that in $La_3Ni_2O_7$ [99–108].

The density-functional-theory (DFT) based calculations suggest that the low-energy degrees of freedom in $La_4Ni_3O_{10}$ are mainly Ni $3d_{z^2}$ and $3d_{x^2-y^2}$ orbitals [99–108]. Similar to $La_3Ni_2O_7$, the interlayer coupling in $La_4Ni_3O_{10}$ is mainly realized through the strong Ni-O-Ni hybridization involving the Ni-$3d_{z^2}$ and O-$p_z$ orbitals [72,73,102]. Such strong interlayer coupling renders that the $3d_{z^2}$ orbital dominant bands are split into the bonding, nonbonding, and antibonding bands [99–108]. Similarly to $La_3Ni_2O_7$, the pressure lifts up the top of the bonding $3d_{z^2}$ band to cross the Fermi level, forming into a hole pocket near the Brillouin zone (BZ) corner $M(\pi, \pi)$ point [99–108], which might be important for the emergence of SC [109]. The antibonding $3d_{z^2}$ component is well above the Fermi level. The nonbonding $3d_{z^2}$ band is a new band absent in $La_3Ni_2O_7$ [99–108]. As this band has a local bottom at the $\Gamma$-point near the Fermi level, different band structures at the $\Gamma$ point may host an electron pocket [103–106] or not [107,108], depending on the band details. This band might also be important for the pairing mechanism [106].

In this Letter, we study the pairing mechanism and pairing symmetry in pressurized $La_4Ni_3O_{10}$ through a standard random-phase-approximation (RPA) approach. We start from

*These authors contributed equally to this work.
†Contact author: chenwq@sustech.edu.cn
‡Contact author: yangfan_blg@bit.edu.cn

 

a six-orbital tight-binding (TB) model fitting our DFT band structure. After adding multiorbital Hubbard interactions, our RPA result provides an $s^{\pm}$-wave SC. The dominant nesting is between the $\gamma$ pocket centering around the $M$ point contributed by the bonding $d_{z^2}$ band and the $\alpha_1$ pocket centering around the $\Gamma$ point contributed by the nonbonding $d_{z^2}$ band. The pairing gap is mainly distributed on the two pockets, with opposite gap signs on them. The real-space pairing pattern is dominated by the interlayer pairing between the $3d_{z^2}$ orbitals in the top and bottom layers within a unit cell. While the pairing symmetry maintains $s^{\pm}$ for low doping levels, the $T_c$ arrives at its maximum at slight electron doping before the system enters the Néel-ordered spin-density-wave (SDW) phase. This $s^{\pm}$ pairing pattern is insensitive to band details.

*Band structure and TB model.* To study the band structure of pressurized $La_4Ni_3O_{10}$, we adopt the tetragonal $I4/mmm$ conventional cell with six Ni atoms. Our DFT calculations utilized the projector-augmented wave (PAW) pseudopotentials with the exchange-correlation of the Perdew-Burke-Ernzerhof and the GGA approach, as implemented in the Vienna *ab initio* Simulation Package (VASP) [110–112]. To account for the correlation effects of $3d$ electrons in Ni atoms, we employed the GGA+$U$ scheme [113], setting $U$ to 3.5 eV [13]. Note that possible local moment fluctuations have been neglected in the DFT+$U$ method, which is left for future study. The cutoff energy for the plane-wave basis was set to 600 eV. The reciprocal space was sampled using a $20\times20\times3$ $k$ mesh for structural optimization and self-consistent calculations. The lattice constants measured experimentally at 40 GPa were utilized [102], and the atomic positions were subsequently relaxed until the atomic force on each atom was less than $10^{-3}$ eV/Å. The obtained band structure is shown in Fig. 1(a), and the density of states (DOS) contributed by different orbital components shown in Fig. 1(b) suggests that the low-energy DOS is mainly contributed by the two Ni-$3d$ orbitals, i.e., $3d_{z^2}$ and $3d_{x^2-y^2}$. The DFT band structure in Fig. 1(a) and the DFT DOS calculation in Fig. 1(b) are both based on the three-dimensional structure, including all possible hoppings in every direction. To acquire a TB description of the DFT band structure, we constructed maximally localized Wannier representations [114] by projecting the Bloch states (with a $20\times20\times3$ $k$ mesh) from the DFT calculations onto the $3d_{z^2}$ and $3d_{x^2-y^2}$ orbitals. As depicted in the Supplemental Material (SM) [115], the band structure obtained from the complete Wannier representations agrees very well with that from DFT calculation across the entire energy range of interest.

To facilitate subsequent studies involving electron interactions, we neglect the coupling between the upper three layers and the lower ones within a unit cell, and by taking each three layers as a unit cell we extract from the Wannier representations the following six-orbital TB model up to the third-nearest-neighbor hopping,

$$H_{\mathrm{TB}} = \sum_{i\mu\sigma} \varepsilon_{i\mu} c^{\dagger}_{i\mu\sigma} c_{i\mu\sigma} + \sum_{ij,\mu\nu,\sigma} t_{ij,\mu\nu} c^{\dagger}_{i\mu\sigma} c_{j\nu\sigma} + \mathrm{H.c.} \quad (1)$$

Here $i/j$ denote combined in-plane coordinate and layer indices, $\mu/\nu$ label orbitals, and $\sigma$ labels spin. $\varepsilon_{i\mu}$ represents the on-site energy of orbital $\mu$ at site $i$. While the full hopping integrals $t_{ij,\mu\nu}$ are provided in the SM [115], only those

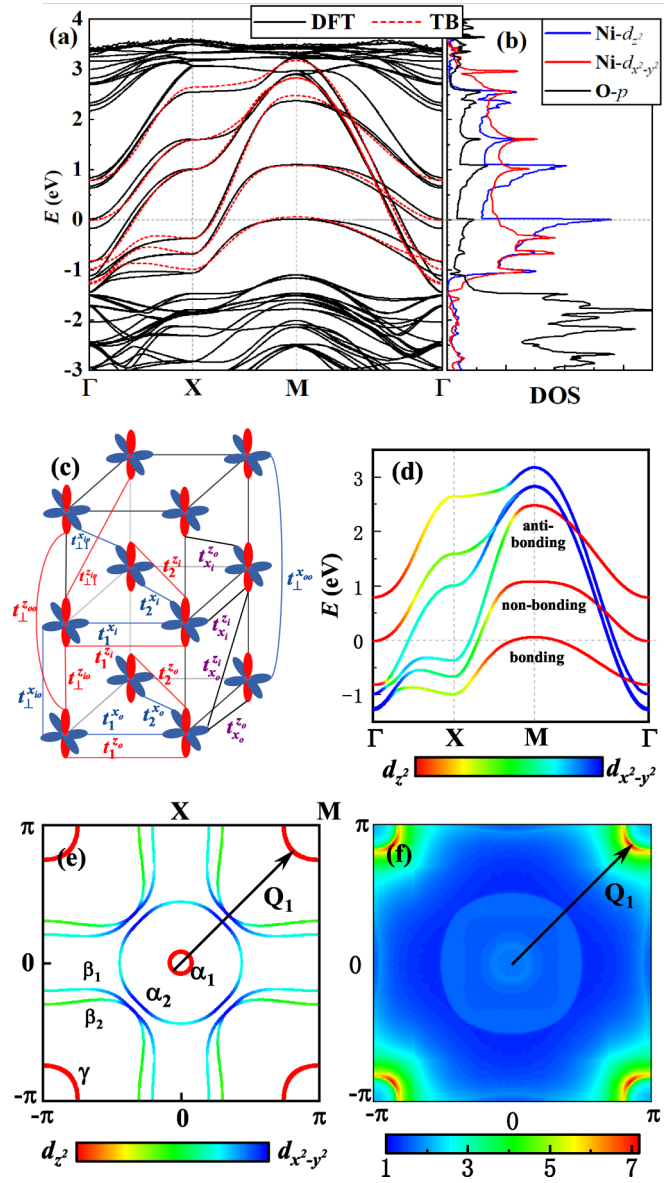


FIG. 1. DFT band structure and six-orbital TB model of pressurized $La_4Ni_3O_{10}$, with experimental refined lattice constants adopted. (a) The DFT (black solid) and six-orbital TB (red dashed) band structure of $La_4Ni_3O_{10}$ under 40 GPa. (b) The DOS for different orbital components of the DFT band in (a). (c) Schematic of the trilayer six-orbital TB model with the hopping integrals marked. The red (blue) pattern represents Ni-$d_{z^2}$($d_{x^2-y^2}$) orbital. (d) The band structure along the high-symmetry lines. (e) FS in the BZ. The five pockets are labeled. The FS-nesting vector is marked by $\mathbf{Q_1}$. The color bar in (d) and (e) indicates the orbital weight of $d_{x^2-y^2}$ and $d_{z^2}$. (f) The distribution of the RPA-renormalized spin susceptibility $\chi^{(s)}(\mathbf{q})$ in the BZ for $U = 1$ eV. The maximum of the distribution locates only at $\mathbf{Q_1}$.

up to the next-nearest-neighbor (NNN) bonds are illustrated in Fig. 1(c). Here the notations $x/z$ indicate $d_{x^2-y^2}/d_{z^2}$ orbitals, $i/o$ represent inner/outer layers, 1/2 indicate NN/NNN intralayer hoppings, and $\perp/\perp1$ mean interlayer hoppings. Similarly to $La_3Ni_2O_7$, the $d_{z^2}$ and $d_{x^2-y^2}$ orbitals dominate the interlayer and intralayer couplings, respectively [74–77].

The obtained band structure for this TB model is shown in Fig. 1(d). A comparison shown in Fig. 1(a) between this band structure and the DFT one suggests that the essential feature of the DFT one has been captured. The associate FS is shown in Fig. 1(e). The strong interlayer hoppings in combination with the weak intralayer hoppings for the $d_{z^2}$ orbital render that the $d_{z^2}$ bands are split into the bonding, nonbonding, and antibonding bands. These $d_{z^2}$-dominant bands are mixed with the $d_{x^2-y^2}$ component through hybridization. The top of the bonding $d_{z^2}$ band crosses the Fermi level, forming the hole-like $\gamma$ pocket centered around the BZ corner $M$ point, as shown in Fig. 1(e). The antibonding $d_{z^2}$ component by itself is completely above the Fermi level (see the red part). Furthermore, it hybridizes with the $d_{x^2-y^2}$ component to form a new band crossing the Fermi level, leading to the hole-like $\beta_1$ pocket around $M$, whose dominant orbital component is $d_{x^2-y^2}$. The nonbonding $d_{z^2}$ band is near the Fermi level and significantly hybridizes with the $d_{x^2-y^2}$ component. This band has a local bottom at the $\Gamma$ point, which slightly crosses the Fermi level, forming the electron-like $\alpha_1$ pocket centered around $\Gamma$. In addition, this band also contributes a large hole-like $\beta_2$ pocket with comparable $d_{z^2}$ and $d_{x^2-y^2}$ components. In comparison with $La_3Ni_2O_7$, the nonbonding $d_{z^2}$ band is new. In addition, an extra electron-like $\alpha_2$ pocket centering around $\Gamma$ is contributed by the $d_{x^2-y^2}$ orbital.

*Interaction and pairing symmetry.* We adopt the following multiorbital Hubbard interaction,

$$H_{int} = U\sum_{i\mu} n_{i\mu\uparrow}n_{i\mu\downarrow} + (U-2J_H)\sum_{i,\sigma,\sigma'} n_{i1\sigma}n_{i2\sigma'} + J_H\sum_{i\sigma\sigma'} \times [c^{\dagger}_{i1\sigma}c^{\dagger}_{i2\sigma'}c_{i1\sigma'}c_{i2\sigma} + (c^{\dagger}_{i1\uparrow}c^{\dagger}_{i1\downarrow}c_{i2\downarrow}c_{i2\uparrow} + \text{H.c.})]. \quad (2)$$

Here, $U$, and $J_H$ denote the Hubbard repulsion, and the Hund's rule coupling (and the pair hopping) respectively. For subsequent calculations, we fix $J_H = U/6$.

We employ the multiorbital RPA approach [116–124] to treat this Hamiltonian, with details provided in the SM [115]. For the present band structure, the critical value of $U$ for the spin-density-wave (SDW) is $U_c \approx 1.2$ eV, which is determined by where the denominator's determinant becomes zero in Eq. (S5) in the SM [115]. And it indicates the onset of magnetic ordering. In the RPA approach, we define the static spin susceptibility matrix $\chi^{(s)}_{\boldsymbol{k}}(pq,st) \equiv \chi^{(s)pq}_{st}(\boldsymbol{k}, i\omega = 0)$, where $\omega$ is the Matsubara frequency. The largest eigenvalue of this Hermitian matrix for each momentum $\boldsymbol{k}$ is defined as $\chi^{(s)}(\boldsymbol{k})$, the largest eigenvalue of the spin susceptibility. The distribution of the spin susceptibility $\chi^{(s)}(\boldsymbol{k})$ over the BZ is shown in Fig. 1(f) for $U = 1$ eV $< U_c$. Notably, the strongest susceptibility locates near the momentum $\mathbf{Q}_1 \approx (\pi, \pi)$, which is the nesting vector between the $\alpha_1$ pocket and $\gamma$ pocket, as shown in Fig. 1(e).

When $U < U_c$, the spin fluctuations can mediate SC, whose $T_c$ is related to the largest pairing eigenvalue $\lambda$ via $T_c \propto e^{-1/\lambda}$, and the pairing symmetry is determined by the corresponding eigenvector. The $U$ dependencies of the largest $\lambda$ for different pairing symmetries, including the $s$ wave, $d_{xy}$ wave, $d_{x^2-y^2}$ wave, and degenerate $(p_x, p_y)$ wave, are shown in Fig. 2(a). Consequently, the $s$ wave is the leading pairing symmetry and dominates other ones, similarly to the case in pressurized $La_3Ni_2O_7$ [78–84]. The calculated pairing

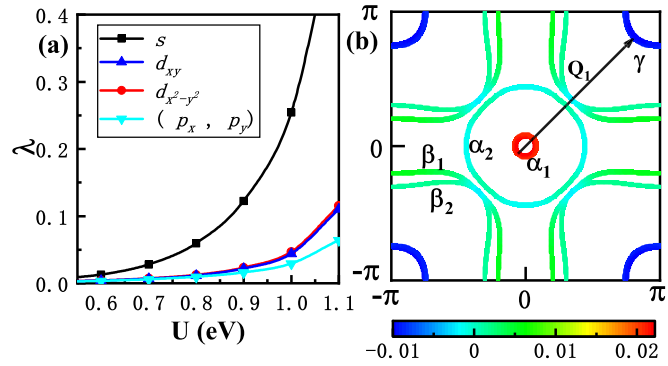


FIG. 2. Pairing eigenvalues λ and leading pairing gap function for undoped $La_4Ni_3O_{10}$ under 40 GPa. (a) The largest λ of the various pairing symmetries as function of $U$ with fixed $J_H = U/6$. (b) Distribution of the leading $s$-wave pairing gap function on the FS for $U = 1$ eV.

eigenvalue λ (∼0.25) of the $s^{\pm}$-wave SC is smaller than that in pressurized $La_3Ni_2O_7$ (∼0.69) for the same $U = 1$ eV [57], which is consistent with experiments. Note that for the simplified two-orbital model adopted here, this $U$ can be different from the bare $U$ employed in the DFT+$U$ calculations [125].

The distribution of the relative gap function is shown on the FS in Fig. 2(b). Consequently, the $\alpha_1$ and $\gamma$ pockets connected by the nesting vector $\mathbf{Q}_1$ are distributed with the strongest pairing amplitude, with their gap signs opposite, forming the $s^{\pm}$-wave pairing similarly to the Fe-based SC [126].

When this $\boldsymbol{k}$-space pairing gap function is Fourier-transformed to the real space, we obtain a dominant interlayer pairing of the $d_{z^2}$ orbitals, as shown in the Fig. 3(a). Since the orbitals in this trilayer system are distinguished as upper, middle, and lower $d_{3z^2-r^2}$, $d_{x^2-y^2}$ orbitals, we classify the pairing components as interlayer [Fig. 3(a)] and intralayer [Fig. 3(b)] pairing. As our results suggest that the interorbital

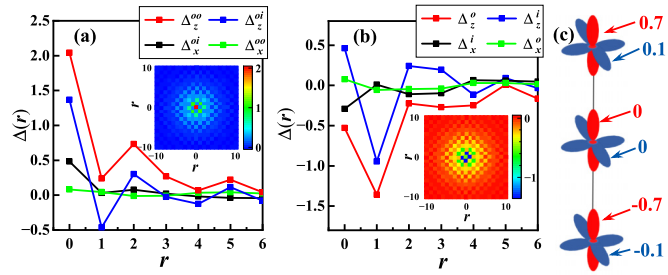


FIG. 3. The real-space pairing pattern and spin-fluctuation pattern. (a), (b) The inter- and intralayer pairing patterns in real space. The main plot shows the distance $r$ dependence of the pairing gap between each two orbitals listed, and the inset shows the spatial distribution of the largest pairing gap among the four listed ones. Here $r$ is the distance in unit cell between the two orbitals involved in the pairing, "oo" means interlayer pairing between the outer and outer layers, "oi" means interlayer pairing between the outer and inner layers, and "o/i" means intralayer pairing within the outer or inner layer. $d_{3z^2-r^2}$ and $d_{x^2-y^2}$ orbitals are represented as "$z$" and "$x$" respectively. (c) The leading spin-fluctuation pattern within a unit cell, in which red (blue) pattern represents Ni-$d_{z^2}$ ($d_{x^2-y^2}$) orbital.

pairing is much weaker than the intraorbital one, we only provide the latter. Figures 3(a) and 3(b) together show that the strongest pairing occurs in the interlayer pairing between the $d_{3z^2-r^2}$ orbitals in the top and bottom outer layers within a unit cell. This is consistent with the fact that the dominant orbital component of the two pockets distributed with the strongest pairing amplitude, i.e., the $\alpha_1$ and $\gamma$ pockets, is $d_{z^2}$. Note that the quasiparticle mass renormalization effects of the shallow Ni-$d_{3z^2-r^2}$ band at the $M$ point are not taken into account. While this effect may influence $T_c$, it is not expected to impact the essential characteristics of the superconducting pairing symmetry and spin susceptibility.

The interlayer pairing for the outer layer–outer layer $d_{3z^2-r^2}$ orbitals is determined by the dominant spin-fluctuation mode which mediates it. While the inter-unit-cell modulation for the dominant spin-fluctuation mode takes the wave vector $\mathbf{Q}_1 \approx (\pi, \pi)$ as suggested by Fig. 1(f), the intra-unit-cell distribution of this mode is depicted in Fig. 3(c). This distribution is determined by the eigenvector corresponding to the largest eigenvalue of the spin-susceptibility matrix defined as $\chi^{(s)}_{p,s} \equiv \chi^{(s)pp}_{ss}(\boldsymbol{k}, i\omega_n = 0)$ with $\boldsymbol{k} = (\pi, \pi)$. Here $\chi^{(s)pp}_{ss}(\boldsymbol{k}, i\omega_n = 0)$ is the element of the spin susceptibility tensor $\chi^{(s)pq}_{st}(\boldsymbol{k}, i\omega_n = 0)$. A remarkable feature of Fig. 3(c) is the strong antiferromagnetic spin correlation between the $d_{z^2}$ orbitals in the top and bottom outer layers, which naturally mediates the interlayer pairing between the $d_{3z^2-r^2}$ orbitals in the top and bottom outer layers, as shown in Fig. 3(a).

*Doping dependence.* The doping $\delta$ dependence of $U_c$ and DOS is shown in Fig. 4(a). The maximal DOS locates at $\delta \approx 0.2$, which takes place when the Fermi level touches the flat bonding $d_{z^2}$ band top. The doping $\delta_{\mathrm{m}}$ for the minimal $U_c$ is slightly lower, which takes place when the $\alpha_1$ and $\gamma$ pockets are best nested to each other with nesting vector $\mathbf{Q}_1 = (\pi, \pi)$. The $\lambda \sim \delta$ relation is shown in Fig. 4(b). With hole doping, the pairing symmetry maintains $s^{\pm}$ but the $\lambda$ and hence $T_c$ obviously drop, while with slight electron doping, the $\lambda$ and hence $T_c$ promptly arise. In a finite doping regime near $\delta_{\mathrm{m}}$, the Néel-ordered SDW emerges for $U = 1$ eV.

The relative gap function for $\delta = 0.05$ is shown in Fig. 4(c). The FS nesting for this doping is much better than that for $\delta = 0$, which is also reflected in the very sharp susceptibility peak at $\mathbf{Q}_1$ displayed in Fig. 4(d), leading to much higher $T_c$. Meanwhile, the $s^{\pm}$ pairing pattern is maintained and is even more obvious. The real-space pairing pattern qualitatively remains unchanged from that for $\delta = 0$ [115], i.e., the interlayer $d_{z^2}$ pairing.

For $\delta = -0.1$, the $\gamma$ pocket is large while the $\alpha_1$ pocket vanishes, as shown in Fig. 4(e) (see the solid lines for the FS). In this case, there is no geometric nesting between the $\gamma$ pocket and the already vanished $\alpha_1$ pocket. However, as the local bottom of the nonbonding $d_{z^2}$ band at the $\Gamma$ point is very close to the Fermi level, there still exists a spin-susceptibility peak at the vector $\mathbf{Q}_1$ connecting the $\Gamma$ point and the boundary of the $\gamma$ pocket, as shown in Fig. 4(f). In this sense, the vector $\mathbf{Q}_1$ can be viewed as a "virtual" nesting vector which works in the pairing pattern. To show the effect of this virtual FS nesting, we provide the distribution of the gap function within an energy shell of $\pm 0.02$ eV around the Fermi level in Fig. 4(e). Consequently, the regime near the $\Gamma$ point still hosts

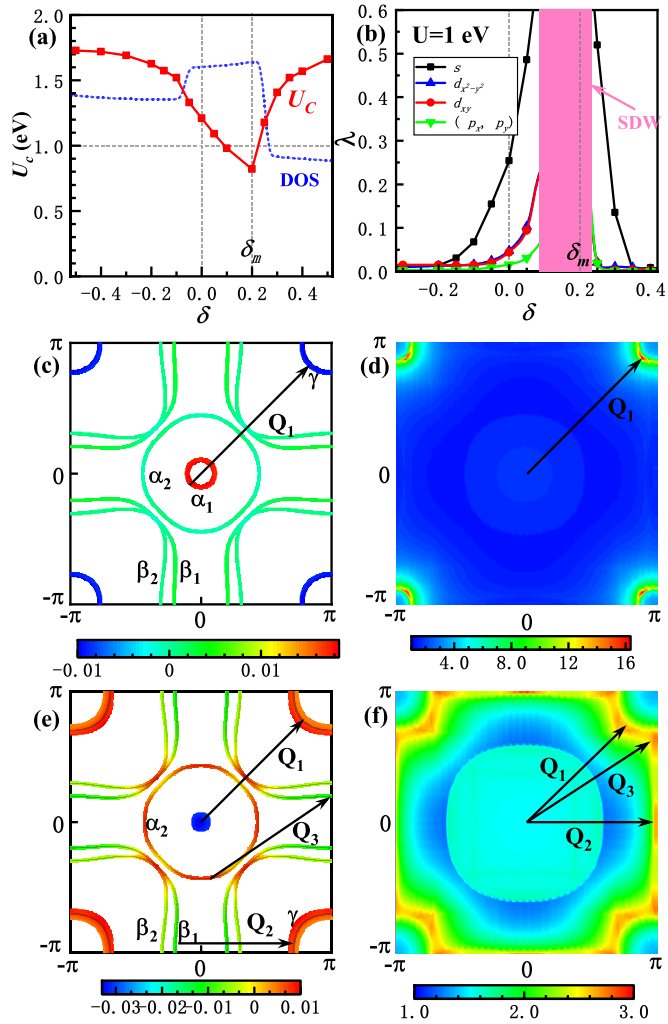


FIG. 4. Doping-dependent study for pressurized $La_4Ni_3O_{10}$. (a) $U_c$ (red solid) and DOS (blue dashed) as functions of the doping $\delta$. (b) The largest pairing eigenvalue $\lambda$ of different pairing symmetries as function of $\delta$. The pink area indicates SDW. (c), (d) Distribution of the leading $s^{\pm}$-wave pairing gap function on the FS (c) and $\chi^{(s)}(\mathbf{q})$ in the BZ (d) for $\delta = 0.05$. The $\mathbf{Q_1}$ in (c) and (d) marks the nesting vector. (e), (f) Distribution of the leading $s$-wave pairing gap function within an energy shell of $\pm 0.02$ eV near the Fermi level (e) and $\chi^{(s)}(\mathbf{q})$ in the BZ (f) for $\delta = -0.1$. In (e) and (f), $\mathbf{Q_1}$ marks the "virtual" nesting vector, and $\mathbf{Q_2}$ and $\mathbf{Q_3}$ are real nesting vectors. In calculating (b)–(f), $U = 1$ eV is adopted.

the largest gap amplitude, with its gap sign opposite to that on the $\gamma$ pocket. Thus we still get the $s^{\pm}$-wave pairing. We also note that for $\delta = -0.1$, two new FS-nesting vectors emerge: the $\mathbf{Q}_2$ between the $\gamma$ and $\beta_1$ pockets, and the $\mathbf{Q}_3$ between the $\alpha_2$ and $\beta_1$ pockets, which are showcased as spin-susceptibility peaks in Fig. 4(f). Consequently, the nested patches between these pockets are also distributed with gap functions with opposite signs, but with weaker amplitude. The real-space pairing pattern qualitatively remains unchanged [115].

*Robust $s^{\pm}$-wave pairing.* As the $\gamma$ and $\alpha_1$ pockets are small, their presence or absence is sensitive to the band-structure details. Figure 5(a) shows the new band structure obtained after the lattice constants and atomic positions of the tetrag-

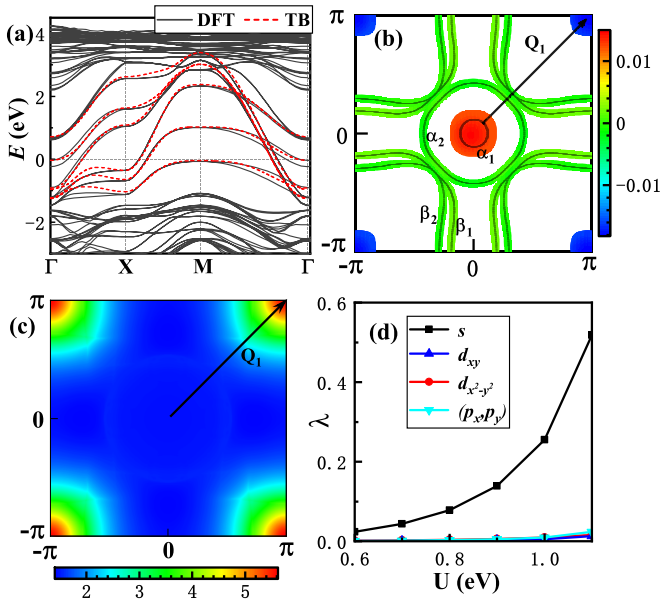


FIG. 5. RPA study based on band structure obtained after the atomic positions and crystal lattices were fully relaxed. (a) The DFT (black solid) and six-orbital TB (red dashed) band structures of $La_4Ni_3O_{10}$ fully relaxed under 40 GPa. (b) Distribution of the leading $s$-wave pairing gap function within an energy shell $\pm 0.03$ eV near the Fermi energy. The FSs are marked by black solid lines. (c) Distribution of $\chi^{(s)}(\mathbf{q})$. In (b) and (c), $\mathbf{Q_1}$ marks the "virtual" nesting vector connecting the boundary of the $\alpha_1$ pocket and the $M$ point. (d) The largest pairing eigenvalue $\lambda$ of the various pairing symmetries as function of the interaction strength $U$ with fixed $J_H = U/6$. In (b) and (c), we adopt $U = 1$ eV.

onal $I4/mmm$ structure are fully relaxed under 40 GPa. The resultant FS is marked by the black solid lines in Fig. 5(b). Different from the previous band structure in Fig. 1(a), this new one hosts the $\alpha_1$ pocket but lacks the $\gamma$ pocket.

Adopting the same Hubbard model (2), we reinvestigate the issue. The obtained $\chi^{(s)}(\boldsymbol{k})$ as shown in Fig. 5(c) still peaks at the "virtual" nesting vector $\mathbf{Q}_1 \approx (\pi, \pi)$ which connects the $M$ point and the boundary of the $\alpha_1$ pocket, as shown in Fig. 5(b). The obtained $U$ dependence of $\lambda$ shown in Fig. 5(d) still yields the $s$ wave as the leading pairing symmetry. The resultant gap function shown in Fig. 5(b) still exhibits the $s^{\pm}$ pattern, wherein the two regimes near the $\Gamma$ and $M$ points host strongest gap functions with opposite signs. The real-space pairing pattern qualitatively maintains unchanged [115]. Therefore, the pairing pattern in this system is insensitive to the band details as well as the slight band dispersion along the $k_z$ direction. While we have not explicitly addressed Hund's rule in constructing our TB models, recent DFT+DMFT studies indicate that Hund's rule coupling does not significantly change the FS shape [103,104], leaving the pairing symmetry and our main conclusions unaffected.

*Conclusion.* Adopting the TB model fitted from the DFT band structure, we have studied the pairing mechanism and pairing symmetry of pressurized $La_4Ni_3O_{10}$ through the RPA approach. Our results provide the $s^{\pm}$-wave pairing driven by spin fluctuations, with a $T_c$ obviously lower than that of pressurized $La_3Ni_2O_7$. The gap amplitude is dominantly distributed at the bottom regime of the nonbonding $d_{z^2}$ band near the $\Gamma$ point and the top regime of the bonding $d_{z^2}$ band near the $M$ point. These two regimes are connected by the nesting vector $\mathbf{Q}_1 \approx (\pi, \pi)$, leading to the opposite gap signs between the two regimes. The real-space pairing pattern is dominated by the interlayer pairing between the $d_{z^2}$ orbitals. This pairing pattern is insensitive to the band-structure details. Upon electron doping, the $T_c$ would increase promptly before the system enters the Néel-ordered spin-density-wave phase.

*Acknowledgments*. We are grateful for discussions with Chen Lu. This work is supported by the NSFC under Grants No. 12234016, No. 12074031, No. 12141402, and No. 12334002, Guangdong province (Grant No. 2020KCXTD001), and Shenzhen Science and Technology Program under Grant No. RCJC20221008092722009. W.-Q.C. is supported by the National Key R&D Program of China (Grant No. 2022YFA1403700), the Science, Technology, and Innovation Commission of Shenzhen Municipality (Grant No. ZDSYS20190902092905285), and the Center for Computational Science and Engineering of Southern University of Science and Technology.

[1] D. Li, K. Lee, B. Y. Wang, M. Osada, S. Crossley, H. R. Lee, Y. Cui, Y. Hikita, and H. Y. Hwang, Superconductivity in an infinite-layer nickelate, Nature (London) **572**, 624 (2019).

[2] D. Li, B. Y. Wang, K. Lee, S. P. Harvey, M. Osada, B. H. Goodge, L. F. Kourkoutis, and H. Y. Hwang, Superconducting dome in $Nd_{1-x}Sr_xNiO_2$ infinite layer films, Phys. Rev. Lett. **125**, 027001 (2020).

[3] S. Zeng, C. S. Tang, X. Yin, C. Li, M. Li, Z. Huang, J. Hu, W. Liu, G. J. Omar, H. Jani, Z. S. Lim, K. Han, D. Wan, P. Yang, S. J. Pennycook, A. T. S. Wee, and A. Ariando, Phase diagram and superconducting dome of infinite-layer $Nd_{1-x}Sr_xNiO_2$ thin films, Phys. Rev. Lett. **125**, 147003 (2020).

[4] M. Osada, B. Y. Wang, B. H. Goodge, K. Lee, H. Yoon, K. Sakuma, D. Li, M. Miura, L. F. Kourkoutis, and H. Y. Hwang, A superconducting praseodymium nickelate with infinite layer structure, Nano Lett. **20**, 5735 (2020).

[5] M. Osada, B. Y. Wang, B. H. Goodge, S. P. Harvey, K. Lee, D. Li, L. F. Kourkoutis, and H. Y. Hwang, Nickelate superconductivity without rare-earth magnetism: (La, Sr)$NiO_2$, Adv. Mater. **33**, 2104083 (2021).

[6] G. A. Pan, D. F. Segedin, H. LaBollita, Q. Song, E. M. Nica, B. H. Goodge, A. T. Pierce, S. Doyle, S. Novakov, D. C. Carrizales, A. T. Niaye, P. Shafer, H. Paik, J. T. Heron, J. A. Mason, A. Yacoby, L. F. Kourkoutis, O. Erten, C. M. Brooks, A. S. Botana *et al.*, Superconductivity in a quintuple-layer square-planar nickelate, Nat. Mater. **21**, 160 (2022).

[7] S. Zeng, C. Li, L. E. Chow, Y. Cao, Z. Zhang, C. S. Tang, X. Yin, Z. S. Lim, J. Hu, P. Yang, and A. Ariando, Superconductivity in infinite-layer nickelate $La_{1-x}Ca_xNiO_2$ thin films, Sci. Adv. **8**, eabl9927 (2022).

[8] Z. Liu, H. Sun, M. Huo, X. Ma, Y. Ji, E. Yi, L. Li, H. Liu, J. Yu, Z. Zhang, Z. Chen, F. Liang, H. Dong, H. Guo, D. Zhong, B. Shen, S. Li, and M. Wang, Evidence for charge and spin density waves in single crystals of $La_3Ni_2O_7$ and $La_3Ni_2O_6$, Sci. China Phys. Mech. Astron. **66**, 217411 (2023).

[9] H. Sun, M. Huo, X. Hu, J. Li, Z. Liu, Y. Han, L. Tang, Z. Mao, P. Yang, B. Wang, J. Cheng, D.-X. Yao, G.-M. Zhang, and M. Wang, Signatures of superconductivity near 80 K in a nickelate under high pressure, Nature (London) **621**, 493 (2023).

[10] J. Hou, P. T. Yang, Z. Y. Liu, J. Y. Li, P. F. Shan, L. Ma, G. Wang, N. N. Wang, H. Z. Guo, J. P. Sun, Y. Uwatoko, M. Wang, G. M. Zhang, B. S. Wang, and J. G. Cheng, Emergence of high-temperature superconducting phase in pressurized $La_3Ni_2O_7$ crystals, Chin. Phys. Lett. **40**, 117302 (2023).

[11] Z. Liu, M. Huo, J. Li, Q. Li, Y. Liu, Y. Dai, X. Zhou, J. Hao, Y. Lu, M. Wang, and H.-H. Wen, Electronic correlations and partial gap in the bilayer nickelate $La_3Ni_2O_7$, Nat. Commun. **15**, 7570 (2024).

[12] Y. Zhang, D. Su, Y. Huang, Z. Shan, H. Sun, M. Huo, K. Ye, J. Zhang, Z. Yang, Y. Xu, Y. Su, R. Li, M. Smidman, M. Wang, L. Jiao, and H. Yuan, High-temperature superconductivity with zero resistance and strange-metal behaviour in $La_3Ni_2O_{7-\delta}$, Nat. Phys. **20**, 1269 (2024).

[13] J. Yang, H. Sun, X. Hu, Y. Xie, T. Miao, H. Luo, H. Chen, B. Liang, W. Zhu, G. Qu, C.-Q. Chen, M. Huo, Y. Huang, S. Zhang, F. Zhang, F. Yang, Z. Wang, Q. Peng, H. Mao, G. Liu *et al.*, Orbital-dependent electron correlation in double-layer nickelate $La_3Ni_2O_7$, Nat. Commun. **15**, 4373 (2024).

[14] M. Zhang, C. Pei, Q. Wang, Y. Zhao, C. Li, W. Cao, S. Zhu, J. Wu, and Y. Qi, Effects of pressure and doping on Ruddlesden-Popper phases $La_{n+1}Ni_nO_{3n+1}$, Mater. Sci. Technol. **185**, 147 (2024).

[15] G. Wang, N. N. Wang, X. L. Shen, J. Hou, L. Ma, L. F. Shi, Z. A. Ren, Y. D. Gu, H. M. Ma, P. T. Yang, Z. Y. Liu, H. Z. Guo, J. P. Sun, G. M. Zhang, S. Calder, J. Q. Yan, B. S. Wang, Y. Uwatoko, and J. G. Cheng, Pressure-induced superconductivity in polycrystalline $La_3Ni_2O_{7-\delta}$, Phys. Rev. X **14**, 011040 (2024).

[16] N. Wang, G. Wang, X. Shen, J. Hou, J. Luo, X. Ma, H. Yang, L. Shi, J. Dou, J. Feng, J. Yang, Y. Shi, Z. Ren, H. Ma, P. Yang, Z. Liu, Y. Liu, H. Zhang, X. Dong, Y. Wang *et al.*, Bulk high-temperature superconductivity in pressurized tetragonal $La_2PrNi_2O_7$, Nature (London) **634**, 579 (2024).

[17] L. Wang, Y. Li, S. Xie, F. Liu, H. Sun, C. Huang, Y. Gao, T. Nakagawa, B. Fu, B. Dong, Z. Cao, R. Yu, S. I. Kawaguchi, H. Kadobayashi, M. Wang, C. Jin, H.-K. Mao, and H. Liu, Structure responsible for the superconducting state in $La_3Ni_2O_7$ at high-pressure and low-temperature conditions, J. Am. Chem. Soc. **146**, 7506 (2024).

[18] Y. Zhou, J. Guo, S. Cai, H. Sun, P. Wang, J. Zhao, J. Han, X. Chen, Q. Wu, Y. Ding, M. Wang, T. Xiang, H.-K. Mao, and L. Sun, Investigations of key issues on the reproducibility of high-$T_c$ superconductivity emerging from compressed $La_3Ni_2O_7$, arXiv:2311.12361.

[19] T. Cui, S. Choi, T. Lin, C. Liu, G. Wang, N. Wang, S. Chen, H. Hong, D. Rong, Q. Wang, Q. Jin, J.-O. Wang, L. Gu, C. Ge, C. Wang, J. G. Cheng, Q. Zhang, L. Si, K. juan Jin, and E.-J. Guo, Strain-mediated phase crossover in Ruddlesden-Popper nickelates, Commun Mater **5**, 32 (2024).

[20] X. Chen, J. Zhang, A. S. Thind, S. Sharma, H. LaBollita, G. Peterson, H. Zheng, D. Phelan, A. S. Botana, R. F. Klie, and J. F. Mitchell, Polymorphism in the Ruddlesden-Popper nickelate $La_3Ni_2O_7$: Discovery of a hidden phase with distinctive layer stacking, J. Am. Chem. Soc. **146**, 3640 (2024).

[21] S. N. Abadi, K.-J. Xu, E. G. Lomeli, P. Puphal, M. Isobe, Y. Zhong, A. V. Fedorov, S.-K. Mo, M. Hashimoto, D.-H. Lu, B. Moritz, B. Keimer, T. P. Devereaux, M. Hepting, and Z.-X. Shen, Electronic structure of the alternating monolayer-trilayer phase of $La_3Ni_2O_7$, arXiv:2402.07143.

[22] P. Puphal, P. Reiss, N. Enderlein, Y.-M. Wu, G. Khaliullin, V. Sundaramurthy, T. Priessnitz, M. Knauft, L. Richter, M. Isobe, P. A. van Aken, H. Takagi, B. Keimer, Y. Suyolcu, B. Wehinger, P. Hansmann, and M. Hepting, Unconventional crystal structure of the high-pressure superconductor $La_3Ni_2O_7$, Phys. Rev. Lett. **133**, 146002 (2024).

[23] H. Wang, L. Chen, A. Rutherford, H. Zhou, and W. Xie, Long-range structural order in a hidden phase of Ruddlesden-Popper bilayer nickelate $La_3Ni_2O_7$, Inorg. Chem. **63**, 5020 (2024).

[24] X. Chen, J. Choi, Z. Jiang, J. Mei, K. Jiang, J. Li, S. Agrestini, M. Garcia-Fernandez, X. Huang, H. Sun, D. Shen, M. Wang, J. Hu, Y. Lu, K.-J. Zhou, and D. Feng, Electronic and magnetic excitations in $La_3Ni_2O_7$, arXiv:2401.12657.

[25] T. Xie, M. Huo, X. Ni, F. Shen, X. Huang, H. Sun, H. C. Walker, D. Adroja, D. Yu, B. Shen, L. He, K. Cao, and M. Wang, Neutron scattering studies on the high-$T_c$ superconductor $La_3Ni_2O_{7-\delta}$ at ambient pressure, arXiv:2401.12635.

[26] M. Xu, S. Huyan, H. Wang, S. L. Bud'ko, X. Chen, X. Ke, J. F. Mitchell, P. C. Canfield, J. Li, and W. Xie, Pressure-dependent "insulator-metal-insulator" behavior in Sr-doped $La_3Ni_2O_7$, Adv. Electron. Mater. **10**, 2400078 (2023).

[27] Z. Dong, M. Huo, J. Li, J. Li, P. Li, H. Sun, Y. Lu, M. Wang, Y. Wang, and Z. Chen, Visualization of oxygen vacancies and self-doped ligand holes in $La_3Ni_2O_{7-\delta}$, Nature (London) **630**, 847 (2024).

[28] D. Zhao, Y. Zhou, M. Huo, Y. Wang, L. Nie, M. Wang, T. Wu, and X. Chen, Spin-density-wave transition in double-layer nickelate $La_3Ni_2O_7$, arXiv:2402.03952.

[29] Y. Cao and Y.-F. Yang, Flat bands promoted by Hund's rule coupling in the candidate double-layer high-temperature superconductor $La_3Ni_2O_7$ under high pressure, Phys. Rev. B **109**, L081105 (2024).

[30] X. Chen, P. Jiang, J. Li, Z. Zhong, and Y. Lu, Critical charge and spin instabilities in superconducting $La_3Ni_2O_7$, arXiv:2307.07154.

[31] Y. Zhang, L.-F. Lin, A. Moreo, and E. Dagotto, Electronic structure, dimer physics, orbital-selective behavior, and magnetic tendencies in the bilayer nickelate superconductor $La_3Ni_2O_7$ under pressure, Phys. Rev. B **108**, L180510 (2023).

[32] Q.-G. Yang, D. Wang, and Q.-H. Wang, Possible $s^{\pm}$-wave superconductivity in $La_3Ni_2O_7$, Phys. Rev. B **108**, L140505 (2023).

[33] F. Lechermann, J. Gondolf, S. Bötzel, and I. M. Eremin, Electronic correlations and superconducting instability in $La_3Ni_2O_7$ under high pressure, Phys. Rev. B **108**, L201121 (2023).

[34] H. Sakakibara, N. Kitamine, M. Ochi, and K. Kuroki, Possible high-$T_c$ superconductivity in $La_3Ni_2O_7$ under high pressure

through manifestation of a nearly half-filled bilayer Hubbard model, Phys. Rev. Lett. **132**, 106002 (2024).

[35] Y. Gu, C. Le, Z. Yang, X. Wu, and J. Hu, Effective model and pairing tendency in bilayer Ni-based superconductor $La_3Ni_2O_7$, arXiv:2306.07275.

[36] Y. Shen, M. Qin, and G.-M. Zhang, Effective bi-layer model Hamiltonian and density-matrix renormalization group study for the high-$T_c$ superconductivity in $La_3Ni_2O_7$ under high pressure, Chin. Phys. Lett. **40**, 127401 (2023).

[37] V. Christiansson, F. Petocchi, and P. Werner, Correlated electronic structure of $La_3Ni_2O_7$ under pressure, Phys. Rev. Lett. **131**, 206501 (2023).

[38] D. A. Shilenko and I. V. Leonov, Correlated electronic structure, orbital-selective behavior, and magnetic correlations in double-layer $La_3Ni_2O_7$ under pressure, Phys. Rev. B **108**, 125105 (2023).

[39] H. Oh and Y.-H. Zhang, Type-II $t$-$J$ model and shared superexchange coupling from Hund's rule in superconducting $La_3Ni_2O_7$, Phys. Rev. B **108**, 174511 (2023).

[40] Z. Liao, L. Chen, G. Duan, Y. Wang, C. Liu, R. Yu, and Q. Si, Electron correlations and superconductivity in $La_3Ni_2O_7$ under pressure tuning, Phys. Rev. B **108**, 214522 (2023).

[41] X.-Z. Qu, D.-W. Qu, J. Chen, C. Wu, F. Yang, W. Li, and G. Su, Bilayer $t$-$J$-$J_\perp$ model and magnetically mediated pairing in the pressurized nickelate $La_3Ni_2O_7$, Phys. Rev. Lett. **132**, 036502 (2024).

[42] Y.-F. Yang, G.-M. Zhang, and F.-C. Zhang, Interlayer valence bonds and two-component theory for high-$T_c$ superconductivity of $La_3Ni_2O_7$ under pressure, Phys. Rev. B **108**, L201108 (2023).

[43] K. Jiang, Z. Wang, and F.-C. Zhang, High-temperature superconductivity in $La_3Ni_2O_7$, Chin. Phys. Lett. **41**, 017402 (2024).

[44] R. Jiang, J. Hou, Z. Fan, Z.-J. Lang, and W. Ku, Pressure driven fractionalization of ionic spins results in cupratelike high-$T_c$ superconductivity in $La_3Ni_2O_7$, Phys. Rev. Lett. **132**, 126503 (2024).

[45] N. Kitamine, M. Ochi, and K. Kuroki, Theoretical designing of multiband nickelate and palladate superconductors with $d^{8+\delta}$ configuration, arXiv:2308.12750.

[46] Z. Luo, B. Lv, M. Wang, W. Wú, and D.-X. Yao, High-$T_c$ superconductivity in $La_3Ni_2O_7$ based on the bilayer two-orbital $t$-$J$ model, npj Quantum Mater. **9**, 61 (2024).

[47] J.-X. Zhang, H.-K. Zhang, Y.-Z. You, and Z.-Y. Weng, Strong pairing originated from an emergent $\mathbb{Z}_2$ Berry phase in $La_3Ni_2O_7$, Phys. Rev. Lett. **133**, 126501 (2024).

[48] Z. Pan, C. Lu, F. Yang, and C. Wu, Effect of rare-earth element substitution in superconducting $R_3Ni_2O_7$ under pressure, Chinese Phys. Lett. **41**, 087401 (2024).

[49] B. Geisler, J. J. Hamlin, G. R. Stewart, R. G. Hennig, and P. J. Hirschfeld, Structural transitions, octahedral rotations, and electronic properties of $A_3Ni_2O_7$ rare-earth nickelates under high pressure, npj Quantum Mater. **9**, 38 (2024).

[50] H. Yang, H. Oh, and Y.-H. Zhang, Strong pairing from a small Fermi surface beyond weak coupling: Application to $La_3Ni_2O_7$, Phys. Rev. B **110**, 104517 (2024).

[51] L. C. Rhodes and P. Wahl, Structural routes to stabilize superconducting $La_3Ni_2O_7$ at ambient pressure, Phys. Rev. Mater. **8**, 044801 (2024).

[52] H. Lange, L. Homeier, E. Demler, U. Schollwöck, F. Grusdt, and A. Bohrdt, Feshbach resonance in a strongly repulsive ladder of mixed dimensionality: A possible scenario for bilayer nickelate superconductors, Phys. Rev. B **109**, 045127 (2024).

[53] H. LaBollita, V. Pardo, M. R. Norman, and A. S. Botana, Electronic structure and magnetic properties of $La_3Ni_2O_7$ under pressure: Active role of the Ni-$d_{x^2-y^2}$ orbitals, arXiv:2309.17279.

[54] U. Kumar, C. Melnick, and G. Kotliar, Softening of $dd$ excitation in the resonant inelastic x-ray scattering spectra as a signature of Hunds coupling in nickelates, arXiv:2310.00983.

[55] T. Kaneko, H. Sakakibara, M. Ochi, and K. Kuroki, Pair correlations in the two-orbital Hubbard ladder: Implications for superconductivity in the bilayer nickelate $La_3Ni_2O_7$, Phys. Rev. B **109**, 045154 (2024).

[56] S. Ryee, N. Witt, and T. O. Wehling, Quenched pair breaking by interlayer correlations as a key to superconductivity in $La_3Ni_2O_7$, Phys. Rev. Lett. **133**, 096002 (2024).

[57] Y. Zhang, L.-F. Lin, A. Moreo, T. A. Maier, and E. Dagotto, Electronic structure, magnetic correlations, and superconducting pairing in the reduced Ruddlesden-Popper bilayer $La_3Ni_2O_6$ under pressure: Different role of $d_{3z^2-r^2}$ orbital compared with $La_3Ni_2O_7$, Phys. Rev. B **109**, 045151 (2024).

[58] H. Schlömer, U. Schollwöck, F. Grusdt, and A. Bohrdt, Superconductivity in the pressurized nickelate $La_3Ni_2O_7$ in the vicinity of a BEC-BCS crossover, arXiv:2311.03349.

[59] J. Chen, F. Yang, and W. Li, Orbital-selective superconductivity in the pressurized bilayer nickelate $La_3Ni_2O_7$: An infinite projected entangled-pair state study, Phys. Rev. B **110**, L041111 (2024).

[60] H. Liu, C. Xia, S. Zhou, and H. Chen, Role of crystal field splitting and long-range hopping on superconducting pairing symmetry of $La_3Ni_2O_7$, arXiv:2311.07316.

[61] Z. Ouyang, J.-M. Wang, J.-X. Wang, R.-Q. He, L. Huang, and Z.-Y. Lu, Hund electronic correlation in $La_3Ni_2O_7$ under high pressure, Phys. Rev. B **109**, 115114 (2024).

[62] X. Sui, X. Han, H. Jin, X. Chen, L. Qiao, X. Shao, and B. Huang, Electronic properties of the bilayer nickelates $R_3Ni_2O_7$ with oxygen vacancies ($R$ = La or Ce), Phys. Rev. B **109**, 205156 (2024).

[63] Y.-Y. Zheng and W. Wú, Superconductivity in the bilayer two-orbital Hubbard model, arXiv:2312.03605.

[64] S. Bötzel, F. Lechermann, J. Gondolf, and I. M. Eremin, Theory of magnetic excitations in the multilayer nickelate superconductor $La_3Ni_2O_7$, Phys. Rev. B **109**, L180502 (2024).

[65] Y. Wang, K. Jiang, Z. Wang, F.-C. Zhang, and J. Hu, The electronic and magnetic structures of bilayer $La_3Ni_2O_7$ at ambient pressure, arXiv:2401.15097.

[66] B. Geisler, L. Fanfarillo, J. J. Hamlin, G. R. Stewart, R. G. Hennig, and P. J. Hirschfeld, Optical properties and electronic correlations in $La_3Ni_2O_7$ bilayer nickelates under high pressure, arXiv:2401.04258.

[67] E. F. Talantsev and V. V. Chistyakov, Debye temperature, electron-phonon coupling constant, and three-dome shape of crystalline strain as a function of pressure in highly compressed $La_3Ni_2O_{7-\delta}$, Lett. Mater. **14**, 262 (2024).

[68] Z. Fan, J.-F. Zhang, B. Zhan, D. Lv, X.-Y. Jiang, B. Normand, and T. Xiang, Superconductivity in nickelate and cuprate su-

perconductors with strong bilayer coupling, Phys. Rev. B **110**, 024514 (2024).

[69] G. Heier, K. Park, and S. Y. Savrasov, Competing $d_{xy}$ and $s\pm$ pairing symmetries in superconducting $La_3Ni_2O_7$: LDA+FLEX calculations, Phys. Rev. B **109**, 104508 (2024).

[70] W.-X. Chang, S. Guo, Y.-Z. You, and Z.-X. Li, Fermi surface symmetric mass generation: A quantum Monte Carlo study, arXiv:2311.09970.

[71] H. Lange, L. Homeier, E. Demler, U. Schollwöck, A. Bohrdt, and F. Grusdt, Pairing dome from an emergent Feshbach resonance in a strongly repulsive bilayer model, arXiv:2309.13040.

[72] Y.-B. Liu, J.-W. Mei, F. Ye, W.-Q. Chen, and F. Yang, $s\pm$-wave pairing and the destructive role of apical-oxygen deficiencies in $La_3Ni_2O_7$ under pressure, Phys. Rev. Lett. **131**, 236002 (2023).

[73] C. Lu, Z. Pan, F. Yang, and C. Wu, Interlayer-coupling-driven high-temperature superconductivity in $La_3Ni_2O_7$ under pressure, Phys. Rev. Lett. **132**, 146002 (2024).

[74] Z. Luo, X. Hu, M. Wang, W. Wu, and D.-X. Yao, Bilayer two-orbital model of $La_3Ni_2O_7$ under pressure, Phys. Rev. Lett. **131**, 126001 (2023).

[75] W. Wú, Z. Luo, D.-X. Yao, and M. Wang, Superexchange and charge transfer in the nickelate superconductor $La_3Ni_2O_7$ under pressure, Sci. China Phys. Mech. Astron. **67**, 117402 (2024).

[76] X.-Z. Qu, D.-W. Qu, W. Li, and G. Su, Roles of Hund's rule and hybridization in the two-orbital model for high-$T_c$ superconductivity in the bilayer nickelate, arXiv:2311.12769.

[77] M. Kakoi, T. Kaneko, H. Sakakibara, M. Ochi, and K. Kuroki, Pair correlations of the hybridized orbitals in a ladder model for the bilayer nickelate $La_3Ni_2O_7$, Phys. Rev. B **109**, L201124 (2024).

[78] C. Lu, Z. Pan, F. Yang, and C. Wu, Interplay of two $E_g$ orbitals in superconducting $La_3Ni_2O_7$ under pressure, Phys. Rev. B **110**, 094509 (2024).

[79] Y. Zhang, L.-F. Lin, A. Moreo, T. A. Maier, and E. Dagotto, Structural phase transition, $s\pm$-wave pairing, and magnetic stripe order in bilayered superconductor $La_3Ni_2O_7$ under pressure, Nat. Commun. **15**, 2470 (2024).

[80] Y. Zhang, L.-F. Lin, A. Moreo, T. A. Maier, and E. Dagotto, Trends in electronic structures and $s\pm$-wave pairing for the rare-earth series in bilayer nickelate superconductor $R_3Ni_2O_7$, Phys. Rev. B **108**, 165141 (2023).

[81] J. Huang, Z. D. Wang, and T. Zhou, Impurity and vortex states in the bilayer high-temperature superconductor $La_3Ni_2O_7$, Phys. Rev. B **108**, 174501 (2023).

[82] Q. Qin and Y.-F. Yang, High-$T_c$ superconductivity by mobilizing local spin singlets and possible route to higher $T_c$ in pressurized $La_3Ni_2O_7$, Phys. Rev. B **108**, L140504 (2023).

[83] Y.-H. Tian, Y. Chen, J.-M. Wang, R.-Q. He, and Z.-Y. Lu, Correlation effects and concomitant two-orbital $s\pm$-wave superconductivity in $La_3Ni_2O_7$ under high pressure, Phys. Rev. B **109**, 165154 (2024).

[84] D.-C. Lu, M. Li, Z.-Y. Zeng, W. Hou, J. Wang, F. Yang, and Y.-Z. You, Superconductivity from doping symmetric mass generation insulators: Application to $La_3Ni_2O_7$ under pressure, arXiv:2308.11195.

[85] S. Abadi, K.-J. Xu, E. G. Lomeli, P. Puphal, M. Isobe, Y. Zhong, A. V. Fedorov, S.-K. Mo, M. Hashimoto, D.-H. Lu, B. Moritz, B. Keimer, T. P. Devereaux, M. Hepting, and Z.-X. Shen, Electronic structure of the alternating monolayer-trilayer phase of $La_3Ni_2O_7$, arXiv:2402.07143.

[86] R. Khasanov, T. J. Hicken, D. J. Gawryluk, L. P. Sorel, S. Bötzel, F. Lechermann, I. M. Eremin, H. Luetkens, and Z. Guguchia, Pressure-induced split of the density wave transitions in $La_3Ni_2O_{7-\delta}$, arXiv:2402.10485.

[87] Y. D. Li, Y. T. Cao, L. Y. Liu, P. Peng, H. Lin, C. Y. Pei, M. X. Zhang, H. Wu, X. Du, W. X. Zhao, K. Y. Zhai, J. K. Zhao, M.-L. Lin, P. H. Tan, Y. P. Qi, G. Li, H. J. Guo, L. Yang, and L. X. Yang, Ultrafast dynamics of bilayer and trilayer nickelate superconductors, arXiv:2403.05012.

[88] S. Rathnayaka, S. Yano, K. Kawashima, J. Akimitsu, C. M. Brown, J. Neuefeind, and D. Louca, Layer buckling and absence of superconductivity in $LaNiO_2$, arXiv:2403.09826.

[89] X.-W. Yi, Y. Meng, J.-W. Li, Z.-W. Liao, W. Li, J.-Y. You, B. Gu, and G. Su, Nature of charge density waves and metal-insulator transition in pressurized $La_3Ni_2O_7$, Phys. Rev. B **110**, L140508 (2024).

[90] S. Wu, Z. Yang, X. Ma, J. Dai, M. Shi, H.-Q. Yuan, H.-Q. Lin, and C. Cao, $Ac_3Ni_2O_7$ and $La_2AeNi_2O_6F$ ($Ae$ = Sr, Ba): Benchmark materials for bilayer nickelate superconductivity, arXiv:2403.11713.

[91] F. Lechermann, S. Bötzel, and I. M. Eremin, Electronic instability, layer selectivity, and Fermi arcs in $La_3Ni_2O_7$, Phys. Rev. Mater. **8**, 074802 (2024)

[92] Z. Ouyang, M. Gao, and Z.-Y. Lu, Absence of electron-phonon coupling superconductivity in the bilayer phase of $La_3Ni_2O_7$ under pressure, npj Quantum Mater. **9**, 80 (2024).

[93] B. V. Beznosikov and K. S. Aleksandrov, Perovskite-like crystals of the Ruddlesden-Popper series, Crystallogr. Rep. **45**, 792 (2000).

[94] P. Lacorre, Passage from T-type to T′-type arrangement by reducing $R_4Ni_3O_{10}$ to $R_4Ni_3O_8$ ($R$ = La, Pr, Nd), J. Solid State Chem. **97**, 495 (1992).

[95] M. Zhang, C. Pei, X. Du, W. Hu, Y. Cao, Q. Wang, J. Wu, Y. Li, H. Liu, C. Wen, Y. Zhao, C. Li, W. Cao, S. Zhu, Q. Zhang, N. Yu, P. Cheng, L. Zhang, Z. Li, J. Zhao *et al.*, Superconductivity in trilayer nickelate $La_4Ni_3O_{10}$ under pressure, arXiv:2311.07423.

[96] Q. Li, Y. Zhang, Z. Xiang, Y. Zhang, X. Zhu, and H.-H. Wen, Signature of superconductivity in pressurized $La_4Ni_3O_{10}$, Chin. Phys. Lett. **41**, 017401 (2024).

[97] Y. Zhu, E. Zhang, B. Pan, X. Chen, D. Peng, L. Chen, H. Ren, F. Liu, N. Li, Z. Xing, J. Han, J. Wang, D. Jia, H. Wo, Y. Gu, Y. Gu, L. Ji, W. Wang, H. Gou, Y. Shen *et al.*, Superconductivity in pressurized trilayer $La_4Ni_3O_{10-\delta}$ single crystals, Nature (London) **631**, 531 (2024).

[98] M. Kakoi, T. Oi, Y. Ohshita, M. Yashima, K. Kuroki, T. Kato, H. Takahashi, S. Ishiwata, Y. Adachi, N. Hatada, T. Uda, and H. Mukuda, Multiband metallic ground state in multilayered nickelates $La_3Ni_2O_7$ and $La_4Ni_3O_{10}$ probed by $^{139}$La-NMR at ambient pressure, J. Phys. Soc. Jpn. **93**, 053702 (2024).

[99] H. Sakakibara, M. Ochi, H. Nagata, Y. Ueki, H. Sakurai, R. Matsumoto, K. Terashima, K. Hirose, H. Ohta, M. Kato, Y. Takano, and K. Kuroki, Theoretical analysis on the possibility of superconductivity in the trilayer Ruddlesden-Popper nickelate $La_4Ni_3O_{10}$ under pressure and its experimental examination: Comparison with $La_3Ni_2O_7$, Phys. Rev. B **109**, 144511 (2024).

[100] H. LaBollita, J. Kapeghian, M. R. Norman, and A. S. Botana, Electronic structure and magnetic tendencies of trilayer $La_4Ni_3O_{10}$ under pressure: Structural transition, molecular orbitals, and layer differentiation, Phys. Rev. B **109**, 195151 (2024).

[101] H. Li, X. Zhou, T. Nummy, J. Zhang, V. Pardo, W. E. Pickett, J. F. Mitchell, and D. S. Dessau, Fermiology and electron dynamics of trilayer nickelate $La_4Ni_3O_{10}$, Nat. Commun. **8**, 704 (2017).

[102] J. Li, C.-Q. Chen, C. Huang, Y. Han, M. Huo, X. Huang, P. Ma, Z. Qiu, J. Chen, X. Hu, L. Chen, T. Xie, B. Shen, H. Sun, D.-X. Yao, and M. Wang, Structural transition, electric transport, and electronic structures in the compressed trilayer nickelate $La_4Ni_3O_{10}$, Sci. China Phys. Mech. Astron. **67**, 117403 (2024).

[103] I. V. Leonov, Electronic structure and magnetic correlations in the trilayer nickelate superconductor $La_4Ni_3O_{10}$ under pressure, Phys. Rev. B **109**, 235123 (2024).

[104] P.-F. Tian, H.-T. Ma, X. Ming, X.-J. Zheng, and H. Li, Effective model and electron correlations in trilayer nickelate superconductor $La_4Ni_3O_{10}$, J. Phys.: Condens. Matter **36**, 355602 (2024).

[105] J.-X. Wang, Z. Ouyang, R.-Q. He, and Z.-Y. Lu, Non-Fermi liquid and Hund correlation in $La_4Ni_3O_{10}$ under high pressure, Phys. Rev. B **109**, 165140 (2024).

[106] Y. Zhang, L.-F. Lin, A. Moreo, T. A. Maier, and E. Dagotto, Prediction of $s\pm$-wave superconductivity enhanced by electronic doping in trilayer nickelates $La_4Ni_3O_{10}$ under pressure, Phys. Rev. Lett. **133**, 136001 (2024).

[107] Q.-G. Yang, K.-Y. Jiang, D. Wang, H.-Y. Lu, and Q.-H. Wang, Effective model and $s\pm$-wave superconductivity in trilayer nickelate $La_4Ni_3O_{10}$, Phys. Rev. B **109**, L220506 (2024).

[108] C.-Q. Chen, Z. Luo, M. Wang, W. Wú, and D.-X. Yao, Trilayer multiorbital models of $La_4Ni_3O_{10}$, Phys. Rev. B **110**, 014503 (2024).

[109] C. Lu, Z. Pan, F. Yang, and C. Wu, Superconductivity in $La_4Ni_3O_{10}$ under pressure, arXiv:2402.06450.

[110] G. Kresse and J. Furthmüller, Efficient iterative schemes for *ab initio* total-energy calculations using a plane-wave basis set, Phys. Rev. B **54**, 11169 (1996).

[111] J. P. Perdew, A. Ruzsinszky, G. I. Csonka, O. A. Vydrov, G. E. Scuseria, L. A. Constantin, X. Zhou, and K. Burke, Restoring the density-gradient expansion for exchange in solids and surfaces, Phys. Rev. Lett. **100**, 136406 (2008).

[112] G. Kresse and D. Joubert, From ultrasoft pseudopotentials to the projector augmented-wave method, Phys. Rev. B **59**, 1758 (1999).

[113] S. L. Dudarev, G. A. Botton, S. Y. Savrasov, C. J. Humphreys, and A. P. Sutton, Electron-energy-loss spectra and the structural stability of nickel oxide: An LSDA+U study, Phys. Rev. B **57**, 1505 (1998).

[114] A. A. Mostofi, J. R. Yates, Y.-S. Lee, I. Souza, D. Vanderbilt, and N. Marzari, wannier90: A tool for obtaining maximally-localised Wannier functions, Comput. Phys. Commun. **178**, 685 (2008).

[115] See Supplemental Material at http://link.aps.org/supplemental/10.1103/PhysRevB.110.L180501 for the comparison between the two band structures obtained from DFT and from the complete Wannier representations, the hopping integrals of the two TB models, the details of the RPA approach, and all the real-space pairing patterns mentioned in the main text.

[116] T. Takimoto, T. Hotta, and K. Ueda, Strong-coupling theory of superconductivity in a degenerate Hubbard model, Phys. Rev. B **69**, 104504 (2004).

[117] K. Yada and H. Kontani, Origin of weak pseudogap behaviors in $Na_{0.35}CoO_2$: Absence of small hole pockets, J. Phys. Soc. Jpn. **74**, 2161 (2005).

[118] K. Kubo, Pairing symmetry in a two-orbital Hubbard model on a square lattice, Phys. Rev. B **75**, 224509 (2007).

[119] K. Kuroki, S. Onari, R. Arita, H. Usui, Y. Tanaka, H. Kontani, and H. Aoki, Unconventional pairing originating from the disconnected Fermi surfaces of superconducting $LaFeAsO_{1-x}F_x$, Phys. Rev. Lett. **101**, 087004 (2008).

[120] S. Graser, T. A. Maier, P. J. Hirschfeld, and D. J. Scalapino, Near-degeneracy of several pairing channels in multiorbital models for the Fe pnictides, New J. Phys. **11**, 025016 (2009).

[121] F. Liu, C.-C. Liu, K. Wu, F. Yang, and Y. Yao, $d + id'$ chiral superconductivity in bilayer silicene, Phys. Rev. Lett. **111**, 066804 (2013).

[122] X. Wu, J. Yuan, Y. Liang, H. Fan, and J. Hu, $g$-wave pairing in $BiS_2$ superconductors, Europhys. Lett. **108**, 27006 (2014).

[123] T. Ma, F. Yang, H. Yao, and H. Q. Lin, Possible triplet $p + ip$ superconductivity in graphene at low filling, Phys. Rev. B **90**, 245114 (2014).

[124] M. Zhang, J.-J. Hao, X. Wu, and F. Yang, Lifshitz transition enhanced triplet $p_z$-wave superconductivity in hydrogen-doped $KCr_3As_3$, Phys. Rev. B **105**, 134509 (2022).

[125] V. Pardo and W. E. Pickett, Metal-insulator transition in layered nickelates $La_3Ni_2O_{7-\delta}$ ($\delta = 0.0, 0.5, 1$), Phys. Rev. B **83**, 245128 (2011).

[126] P. J. Hirschfeld, M. M. Korshunov, and I. I. Mazin, Gap symmetry and structure of Fe-based superconductors, Rep. Prog. Phys. **74**, 124508 (2011).